

# MULTIEDITS: SIMULTANEOUS MULTI-ASPECT EDITING WITH TEXT-TO-IMAGE DIFFUSION MODELS

Mingzhen Huang, Jialing Cai, Shan Jia, Vishnu Suresh Lokhande, Siwei Lyu  
 Department of Computer Science, University at Buffalo, State University of New York, USA

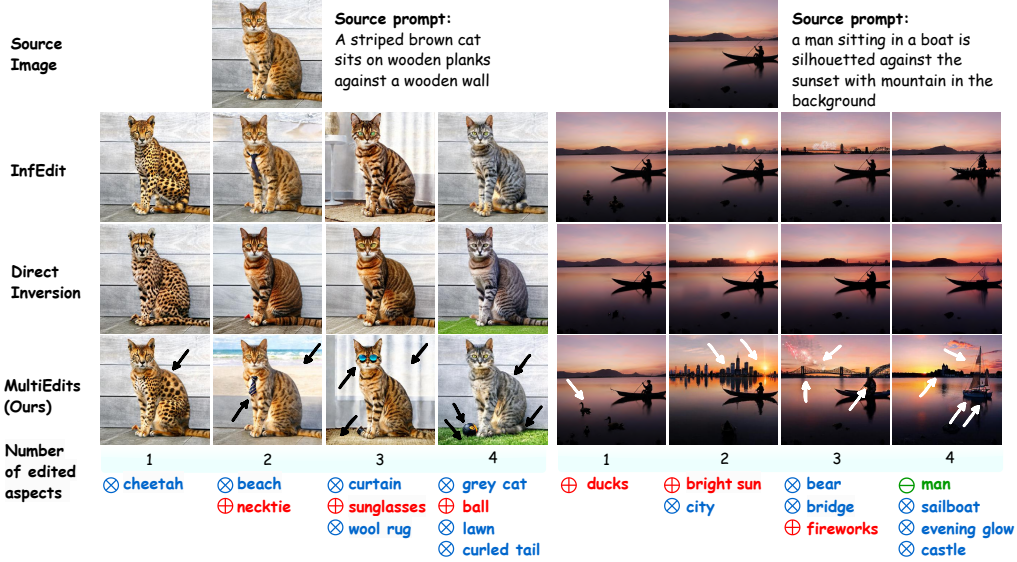


Figure 1: **Multi-aspect text-driven image editing.** Editing multiple attributes or aspects in images presents a significant challenge for existing models, such as DirectInversion (Ju et al., 2023) and InfEdit (Xu et al., 2023), as their performance degrades with an increasing number of aspects. In contrast, our MultiEdits method can achieve precise multi-aspect image editing in 5 seconds. Here, the symbol  $\otimes$  denotes an aspect or attribute swap action from the source prompt,  $\oplus$  denotes an aspect addition action to the source prompt, and  $\ominus$  denotes an aspect deletion from the source prompt. Arrows ( $\rightarrow$ ) on the image highlight the aspects edited by our method.

## ABSTRACT

Text-driven image synthesis has made significant advancements with the development of diffusion models, transforming how visual content is generated from text prompts. Despite these advances, text-driven image editing, a key area in computer graphics, faces unique challenges. A major challenge is making simultaneous edits across multiple objects or attributes. Applying these methods sequentially for multi-aspect edits increases computational demands and efficiency losses. In this paper, we address these challenges with significant contributions. Our main contribution is the development of MultiEdits, a method that seamlessly manages simultaneous edits across multiple attributes. In contrast to previous approaches, MultiEdits not only preserves the quality of single attribute edits but also significantly improves the performance of multitasking edits. This is achieved through innovative attention distribution mechanism and multi-branch design that operates across several processing heads. Additionally, we introduce the PIE-Bench++ dataset, an expansion of the original PIE-Bench dataset, to better support evaluating image-editing tasks involving multiple objects and attributes simultaneously. This dataset is a benchmark for evaluating text-driven image editing methods in multifaceted scenarios. Dataset and code is available at <https://mingzhenhuang.com/projects/MultiEdits.html>

---

## 1 INTRODUCTION

Recently, text-driven image editing has experienced remarkable growth, driven by advances in diffusion-based image generative models. This technique involves modifying existing images based on textual prompts to alter objects, their attributes, and the relationships among various objects. The latest methods (Hertz et al., 2022; Ju et al., 2023; Cao et al., 2023) can produce edited images that closely match the semantic content described in the prompts while keeping the rest of the image unchanged. Unlike early image editing approaches that required image matting to precisely extract foreground objects using alpha mattes (Li et al., 2023), text-driven editing offers a less labor-intensive alternative. User-provided textual prompts guide the edits, with auxiliary inputs like masks facilitating localized modifications (Liu et al., 2021).

While these methods have showcased promising results, existing methods typically focus on editing a single aspect in the source image. An “aspect” refers to a specific attribute or entity within the textual prompt that describes the image and can be modified, such as object type, color, material, pose, or relationship. The ability to edit multiple aspects (Chang et al., 2024; Joseph et al., 2024) through text prompts has not been extensively explored. We introduce the concept of *multi-aspect text-driven image editing* to address this gap. Multi-aspect image editing is essential due to the rich and diverse content and structure of digital images, as well as the varied requirements of users. For example, it always occurs that users wish to modify multiple attributes or regions in an image, such as adding a necktie to a cat and changing the background wall to a beach (Fig. 1, Left), or removing a man and replacing a mountain with a castle in the right example. Unlike traditional editing methods (e.g., (Ju et al., 2023; Xu et al., 2023)) that focus on a single aspect, multi-aspect editing allows users to manipulate various aspects simultaneously. Unlike text-to-image synthesis (Gu et al., 2022; Ding et al., 2022), which generates content entirely from scratch, multi-aspect editing operates on the existing source image, ensuring the preservation of essential content. It bridges the gap between single-aspect editing and full synthesis, accommodating a diverse array of editing scenarios.

However, we observe that directly applying the single-aspect text-driven image editing methods in cases where multiple image aspects must be modified often does not yield satisfactory results. A straightforward solution to this problem is to apply the single aspect editing method *sequentially* – we can order the aspects to be modified and use a single-aspect editing method to change the aspects one by one. Although sequential applications of single-aspect text-driven image editing methods can modify multiple aspects of an image, they may introduce significantly higher computational overhead. More importantly, the order of the aspects modified may affect the quality – changes to later aspects may undo the early ones or accumulate the errors and artifacts, thus reducing the effectiveness of the final editing results, as the last two rows of Fig. 5 and Table 1 show.

In this work, we introduce *MultiEdits* as an efficient and effective solution to the problem of multi-aspect text-driven image editing. This method is based on a crucial insight that the editing step can occur in parallel with the image’s diffusion steps. Therefore, in MultiEdits, aspect editing is conducted at every diffusion step to accelerate the editing process. *ParallelEdits* is based on an architecture with a fixed number of additional branches dedicated to handling rigid, non-rigid, and style changes. This design ensures scalability independent of the number of prompt aspects altered. In addition, we employ an attention aggregator to accurately assess editing difficulty and route aspects to appropriate branches within the MultiEdits framework, ensuring precise and efficient editing. To enable subsequent research and evaluation of multi-aspect text-driven image editing methods, we also build the PIE-Bench++ dataset, an extension of the PIE-Bench (Ju et al., 2023) that has 700 images with detailed text prompts and tailored to facilitate simultaneous edits across multiple image aspects. We propose evaluation metrics and benchmark different text-driven image editing methods on PIE-Bench++. MultiEdits outperforms the state-of-the-art image editing methods on PIE-Bench++.

## 2 RELATED WORKS

**Diffusion Models for Text-Driven Image Editing.** Text-driven image editing focuses on modifying specific areas of an image according to textual prompts. The primary objectives of this editing process are twofold: to ensure the modifications accurately reflect the given instructions and to maintain the integrity of the essential content. Diffusion models (Rombach et al., 2022) have gained

---

popularity as a preferred image editing model for their capacity for generating high-quality samples by incorporating diverse conditions, especially using text (Couairon et al., 2023; Parmar et al., 2023; Xu et al., 2023; Kawar et al., 2023; Couairon et al., 2022; Nguyen et al., 2023; Ju et al., 2023). This involves transforming the images into the latent space and generating regions using diffusion models conditioned by the text prompt while ensuring accurate reconstruction of unmodified regions during editing. To avoid the edited image deviating from original image, early text-driven image editing typically requires user-specified masks as additional condition (Lugmayr et al., 2022; Avrahami et al., 2022; Nichol et al., 2021) or training (Choi et al., 2021; Xu et al., 2024; Zhao et al., 2022) to guided the editing process, which constrain their potential application. To address this limitation, recent editing models, such as InfEdit (Xu et al., 2023), PnP (Tumanyan et al., 2023), Direct Inversion (Ju et al., 2023) follow the work Prompt-to-Prompt (P2P) (Hertz et al., 2022), which proposed to obtain an attention map from the cross attention process and either swap or refine the attention map from text prompt for image editing. This design automatically obtains the editing mask and only allows image editing using a text prompt. Another method, MasaCtrl (Cao et al., 2023), converts existing self-attention in diffusion models into mutual self-attention for non-rigid consistent image synthesis and editing, enabling to query correlated local contents and textures from source images for consistency.

**Multi-Aspect Image Editing.** Current image editing models demonstrate promising results in text-driven image editing benchmarks. However, these models excel at single-attribute editing but encounter significant challenges when tasked with editing multiple attributes (Chang et al., 2024; Joseph et al., 2024), particularly when involving multiple objects (as shown in Fig. 1). We attribute this limitation to the following reasons. First, existing methods use the attention mask to direct where edits should be made. With multiple attributes, the editing area may expand significantly, incorporating extensive semantic information or scattered regions that are challenging to edit using a single mask. Second, employing a fixed mask from cross-attention maps struggles with edits involving changes in region size (such as pose adjustments), while using an adaptive mask faces challenges in maintaining edit fidelity. Therefore, integrating various attention masks for accurate multi-attribute editing presents a challenging technical problem. Early studies (Wang et al., 2022; Khodadadeh et al., 2022) have employed GAN models such as StyleGAN2 (Karras et al., 2020) to edit multiple attributes in faces. The multiple-attribute editing is realized by training the GAN model with supervised multi-class training and a training dataset of image and attribute vector pairs. The solution heavily relies on the training sets and has limitations in generalizing to new editing types. Few recent works achieve multi-aspect editing with additional inputs: (Ge et al., 2023) leverages rich text to edit multiple objects and (Chang et al., 2024) pre-processes the image with grounding to localize multiple edited regions for multi-aspect editing. However, the editing performance highly relies on additional input beyond plain text, either from user input or other off-the-shelf models. A recent work (Joseph et al., 2024) proposes an iterative multi-granular image editor, where a diffusion model can faithfully follow a series of image editing instructions from a user. However, this interactive editing pipeline will result in significant computational overhead.

**Image Editing with Multiple Branches.** In the literature (Cao et al., 2023; Hertz et al., 2022), image editing processes have been conducted by implementing a dual-branch approach. This methodology involves segregating source and target branches throughout the editing process. Specifically, the source branch is reverted to the original image, while the trajectory of the target branch is iteratively adjusted. Calibration of the target branch is achieved at each time-step by computing the distance from the source branch. Our observation underscores the disparity between the effectiveness of a dual branch in enhancing the editing process and its failure in multi-aspect editing. A singular target branch proves inadequate in calibrating fully from the source branch, leading to imperfect incorporation of all aspects into the image. Hence, our primary proposition advocates for multi-aspect editing by utilizing multiple target branches. Each target branch’s trajectory is meticulously calibrated, with simpler concepts addressed in the initial branches and more complex aspects deferred to subsequent ones. In the following section, we will delve deeper into this concept.

### 3 DIFFUSION-BASED IMAGE GENERATION AND EDITING

We are provided with an image sample  $x_0$  which transforms the latent space via an encoder/decoder pair  $\mathcal{E}/\mathcal{D}$ , such that  $z_0 = \mathcal{E}(x_0)$ . Here,  $z_0$  represents the latent representation of the image  $x_0$ . With a slight abuse of notation, we approximate the reconstructed image  $\bar{x}_0$  as  $\mathcal{D}(\bar{z}_0)$ , where  $\bar{z}_0$

denotes the reconstructed version of  $z_0$ . These operations are integral to the latent diffusion model (Rombach et al., 2022). The diffusion process constitutes two steps: the forward step incrementally adds zero-mean white Gaussian noise with time-varying variance to the latent vector  $z$  according to discrete-time  $t^*$ ,

$$z_t = \sqrt{\alpha_t} z_0 + \sqrt{1 - \alpha_t} \epsilon \quad \text{with } \epsilon \sim \mathcal{N}(0, I), \quad (1)$$

$\alpha_{1:T}$  represents a variance schedule for  $t$  drawn from the interval  $[1, T]$ . The variance schedule can be different, such as linear or cosine quadratic (Nichol & Dhariwal, 2021). The backward step is an iterative process to remove the noise from the data progressively. Using the same variance schedule  $\alpha_{1:T}$  as in the forward step, a noise schedule  $\sigma_{1:T}$  and a parameterized noise prediction network  $\epsilon_\theta$  with coefficients  $c_{\text{pred}} = \sqrt{\alpha_{t-1}}$ ,  $c_{\text{dir}} = \sqrt{1 - \alpha_{t-1} - \sigma_t^2}$ , and  $c_{\text{noise}} = \sigma_t$ , the backward step corresponds to the following process:

$$z_{t-1} = \underbrace{c_{\text{pred}} f_\theta(z_t, t)}_{\text{predicting } \bar{z}_0} + \underbrace{c_{\text{dir}} \epsilon_\theta(z_t, t)}_{\text{adjust along } z_t} + \underbrace{c_{\text{noise}} \epsilon_t}_{\text{random noise}} \quad \text{with } \epsilon_t \sim \mathcal{N}(0, I) \quad (2)$$

The noise schedule  $\sigma_{1:T}$  comprises hyperparameters requiring careful selection based on factors like image dimensions or desired performance (Chen, 2023)(Karras et al., 2022). In the framework of Denoising Diffusion Implicit Models (DDIM) (Song et al., 2020), the function  $f_\theta$  is employed for the prediction and reconstruction of  $\bar{z}_0$ , based on the input  $z_t$ . Specifically, we have  $\bar{z}_0 = f_\theta(z_t, t) = \frac{1}{\sqrt{\alpha_t}} z_t - \frac{\sqrt{1 - \alpha_t}}{\sqrt{\alpha_t}} \epsilon_\theta(z_t, t)$ .

**Consistency Models for Inversion-free Image Editing.** Consistency models (Song et al., 2023; Luo et al., 2023) have been introduced to expedite the generation process through a consistent distillation approach. These models exhibit a self-consistency property, ensuring that samples along the same trajectory map to the same initial point. Specifically, the function  $f_\theta$  is rendered self-consistent by satisfying  $f_\theta(z_t, t) = z_0$  for a given sample  $z_t$  at timestep  $t$ . As a result, the self-consistency property yields a closed-form solution for the noise predictor  $\epsilon_\theta$ . We denote this particular  $\epsilon_\theta$  as  $\epsilon^{\text{cons}}$ , which is derived as  $\epsilon^{\text{cons}} = \frac{z_t - \sqrt{\alpha_t} z_0}{\sqrt{1 - \alpha_t}}$ . Since  $\epsilon^{\text{cons}}$  is not parameterized and contains the ground-truth  $z_0$ , Xu et al. [3] propose starting directly with random noise, i.e.,  $z_T \sim \mathcal{N}(0, \mathbf{I})$ , at the last time-step  $T$ , which is particularly advantageous for image-editing tasks as it eliminates the need for inversion from  $z_0$  to  $z_T$ . Therefore, starting with  $z_\tau = z_T \sim \mathcal{N}(0, \mathbf{I})$ , the sampling process proceeds as follows:

- ①  $z = \frac{z_\tau - \sqrt{1 - \alpha_\tau} \epsilon_\tau^{\text{cons}}}{\sqrt{\alpha_\tau}}$ . Where,  $\epsilon_\tau^{\text{cons}}$  is given by  $\frac{z_\tau - \sqrt{\alpha_\tau} z_0}{\sqrt{1 - \alpha_\tau}}$
- ② Noise is added to  $z_\tau$ , i.e.,  $z_\tau = \sqrt{\alpha_\tau} z + \sqrt{1 - \alpha_\tau} \epsilon$  where  $\epsilon \sim \mathcal{N}(0, \mathbf{I})$

After many iterations, the final output is  $z$ . Furthermore, (Xu et al., 2023) demonstrates that the dual-branch paradigm (involving a source and a target branch) used in image editing tasks can be executed in an inversion-free manner. We will delve into this, along with our method description, in Section 4.2.2.

## 4 MULTI-ASPECT IMAGE EDITING

### 4.1 PROBLEM DEFINITION

The input to the multi-aspect image editing task includes a source image ( $\mathcal{I}_{\text{src}}$ ), the source prompt, and a set of edits to be applied to the source image, indicating the changes from the source prompt to target prompt. A text prompt (whether source or target) comprises several independent tokens, of which only a subset is editable. We refer to these editable tokens as *Aspects*.

**Definition 4.1** (Aspect). We define an  $i^{\text{th}}$  aspect  $\mathcal{A}_{\text{src}}^i$  in the source prompt (or the  $j^{\text{th}}$  aspect  $\mathcal{A}_{\text{edt}}^j$  in the target prompt) as any entity that can be substituted, deleted, or inserted into the text prompt, maintaining a meaningful sentence structure.

Several examples of tokens corresponding to aspects or not are given in Fig. 3. In other words, aspects correspond to single or multiple tokens representing object color, pose, material, content,

\*Diffusion process is rigorously defined as a continuous-time stochastic differential equation, but in practice often implemented with discrete-time updates.

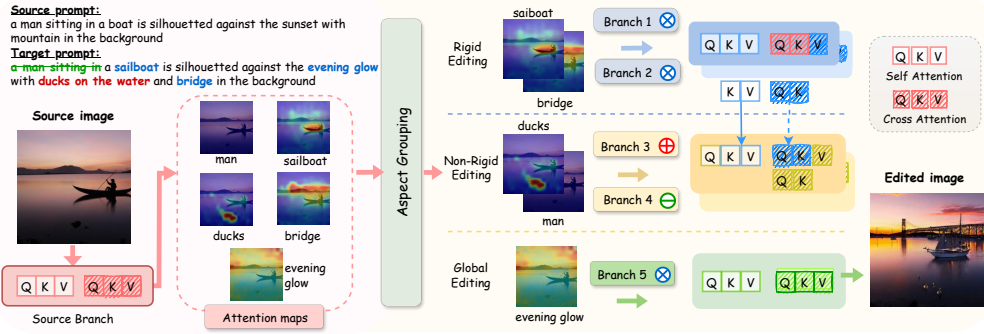


Figure 2: **Pipeline.** Our method, MultiEdits, takes a source image, source prompt, and target prompt as input and produces an edited image. The target prompt specifies the edits needed in the source image. Attention maps for all edited aspects are first collected. Aspect Grouping (see Section 4.2.1) categorizes each aspect into one of  $N$  groups (in the above figure,  $N = 5$ ). Each group is then assigned a branch and the branch-level updates are detailed in Section 4.2.2. Each branch can be viewed either as a rigid editing branch, non-rigid editing branch, or global editing branch. Finally, adjustments to query/key/value at the self-attention and cross-attention layers are made, as illustrated in the figure and described in Section 4.2.3.

background, image style, etc. An editing operation between a pair of tokens ( $\mathcal{A}_{src}^i, \mathcal{A}_{edt}^j$ ) is defined as  $E^{i \rightarrow j} \in \{\otimes, \oplus, \ominus, \emptyset\}$ . Here,  $\otimes$  denotes a swap action,  $\oplus$  denotes an object addition action,  $\ominus$  denotes object deletion, and  $\emptyset$  indicates no change in the aspect. Such an editing operation can be inferred directly by appropriately mapping the source and target prompts, or it can be provided as metadata (Hertz et al., 2022; Mokady et al., 2023). The editing task is considered successful if the edited source image,  $\mathcal{I}_{edt}$ , reflects the required edits while preserving the unaffected aspects of the original image.

## 4.2 METHOD

Figure 2 outlines the overall pipeline of our method, which has three steps. In the first step (Sec. 4.2.1), we perform *aspect grouping* using attention maps generated by running a few iterations of the diffusion process conditioned on source prompt and target prompt. The aspects in the target image are put into up to  $N$  groups, each processed by a distinct branch. The second step (Sec. 4.2.2) demonstrates how each branch, which receives a specific group of aspects, performs inversion-free editing. In the last step (Sec. 4.2.3), we perform the necessary adjustments for enabling cross-branch interaction and elucidate the significance of such interaction.

### 4.2.1 ASPECT GROUPING

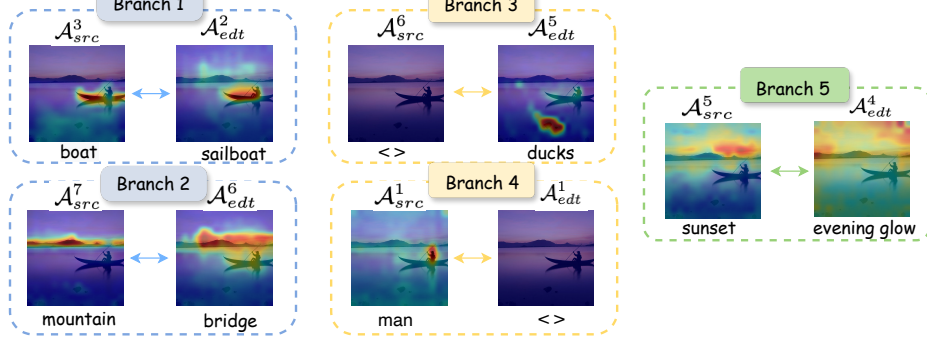
We would like to group aspects in a prompt into  $N$  distinct groups using the cross-attention maps of the diffusion UNet (Ronneberger et al., 2015) to characterize the spatial layouts as in previous studies (Tang et al., 2022). Given an editing operation  $E^{i \rightarrow j}$  between the source aspect  $\mathcal{A}_{src}^i$  and the target aspect  $\mathcal{A}_{edt}^j$ , we obtain the corresponding attention maps from both the source and target prompts as  $\bar{\mathcal{M}}_{src}^i$  and  $\bar{\mathcal{M}}_{edt}^j$ , respectively. The attention map  $\mathcal{M}$  is defined by the query feature  $\hat{Q}$  and key feature  $\hat{K}$  from the cross-attention as  $\mathcal{M} = \text{softmax} \left( \frac{\hat{Q}\hat{K}^T}{\sqrt{d}} \right)$ . The binarized attention map  $\bar{\mathcal{M}}$  is obtained by normalizing  $\mathcal{M}$  and thresholding its values. Our aspect grouping proceeds in two steps, **Step (A). Assign a type for every editing operation ( $E^{i \rightarrow j}$ )**. We consider three possible types of edits, in line with previous works (Cao et al., 2023), namely a global edit, a local rigid edit or a local non-rigid edit. Rigid local edits, such as changing an object’s color or texture, do not alter the layout of objects. Conversely, non-rigid local edits modify the layout of objects, such as adding or deleting objects or changing object poses. Global edits affect background and style changes. The type assignment for the editing operation ( $E^{i \rightarrow j}$ ) is determined by the following rules:

$$\text{type}(E^{i \rightarrow j}) = \begin{cases} \text{global edit} & \dots \dots \dots \gamma(\bar{\mathcal{M}}_{edt}^j) \geq \beta \gamma(\sum \bar{\mathcal{M}}_{edt}) \\ \text{non-rigid edit} & \phi(\bar{\mathcal{M}}_{src}^i, \bar{\mathcal{M}}_{edt}^j) < \lambda \\ \text{rigid edit} & \phi(\bar{\mathcal{M}}_{src}^i, \bar{\mathcal{M}}_{edt}^j) \geq \lambda \end{cases} \text{local edit} \dots \gamma(\bar{\mathcal{M}}_{edt}^j) < \beta \gamma(\sum \bar{\mathcal{M}}_{edt}) \quad (3)$$

**Source prompt:**

a man sitting in a boat is silhouetted against the sunset with mountain in the background

$$\mathcal{A}_{src}^1 \mathcal{A}_{src}^2 \quad \mathcal{A}_{src}^3 \quad \mathcal{A}_{src}^4 \quad \mathcal{A}_{src}^5 \quad \mathcal{A}_{src}^7 \quad \mathcal{A}_{src}^8$$



**Target prompt:**

a man sitting in a sailboat is silhouetted against the evening glow with ducks on the water and bridge in the background

$$\mathcal{A}_{edt}^1 \quad \mathcal{A}_{edt}^2 \quad \mathcal{A}_{edt}^3 \quad \mathcal{A}_{edt}^4 \quad \mathcal{A}_{edt}^5 \quad \mathcal{A}_{edt}^6 \quad \mathcal{A}_{edt}^7$$

Figure 3: **Aspects and Aspect Grouping.** In a text prompt, there are multiple independent tokens, with only some being editable, known as aspects and are underlined in the above example. These aspects can be added, deleted, or swapped between the source and target prompts. Pairs of source and target aspects are grouped into branches, and the methodology for aspect grouping is explained in Section 4.2.1.

Here,  $\phi$  represent mIoU (Lin et al., 2014), while  $\gamma$  indicates the alpha mattes of attention maps.  $\lambda$  and  $\beta$  are tunable hyperparameters. For further details, please refer to the supplementary Sec. E.

**Step (B). Categorize every editing operation ( $E^{i \rightarrow j}$ ) into  $N$  groups.** For each editing operation ( $E^{i \rightarrow j}$ ) of a specific type, we assess whether  $\phi(\bar{\mathcal{M}}_{edt}^j, \bar{\mathcal{M}}_{edt}^k) \geq \lambda$  to determine if there exists substantial overlap between any pair of attention maps of that type. If significant overlap is detected, the attention maps are grouped together. On the other hand, if attention maps are isolated like the "boat" and "mountain" in Fig. 3 are categorized into separate groups due to small overall. Therefore, we have a total of  $N$  groups. Each group has a dedicated branch, resulting in a total of  $N > 2$  branches.

#### 4.2.2 INVERSION-FREE MULTI-BRANCH EDITING

We use a set of  $N$  branches indexed by  $n$ . These  $N$  branches are in addition to a source branch (also shown in Figure 2) that undergoes a DDCM sampling process (Xu et al., 2023). The  $n^{\text{th}}$  branch is calibrated to its  $(n-1)^{\text{th}}$  branch, and the first branch is calibrated to the source branch. The  $N$ -way target branch calibration can occur simultaneously, saving significant compute time. For the DDCM sampling process of the  $n^{\text{th}}$  branch, it has the form of Section 3, Step ①:

$$\underbrace{z(n)^{\text{edt}}}_{\text{edited latent}} = \left( \underbrace{z(n)_{\tau}^{\text{edt}}}_{\text{noisy latent}} - \sqrt{1 - \alpha_{\tau}} \left( \underbrace{\epsilon(n)_{\tau}^{\text{edt}}}_{\text{parameterized noise}} - \underbrace{\epsilon(n-1)_{\tau}^{\text{edt}}}_{\text{consistency noise}} \right) \right) / \sqrt{\alpha_{\tau}} \quad (4)$$

Let us break down Eq. 4 step by step.  $n = 0$  representing the source branch, we have  $z(0)^{\text{edt}} = z^{\text{src}}$  and  $\epsilon(0)_{\tau}^{\text{edt}} = \epsilon_{\tau}^{\text{src}}$ . Also,  $z(0)_{\tau}^{\text{edt}} = z_{\tau}^{\text{src}}$ , which at time step  $\tau = \tau_1$ , is random noise drawn from  $\mathcal{N}(0, \mathbf{I})$ . Similarly, when  $n = N$ ,  $z(N)^{\text{edt}}$  represents the final calibrated/edited image containing all the required aspect edits after repeating for  $\tau \in \{\tau_1, \tau_2, \dots, \tau_T\}$  timesteps. The noise addition on any target branch remains the same as Step ②, i.e.,  $z(n)_{\tau}^{\text{edt}} = \sqrt{\alpha_{\tau}} z(n)^{\text{edt}} + \sqrt{1 - \alpha_{\tau}} \epsilon$  where  $\epsilon \sim \mathcal{N}(0, \mathbf{I})$ . For  $0 \leq n \leq N$ , we have  $\epsilon(n)_{\tau}^{\text{edt}} = \epsilon_{\theta}(z(n)_{\tau}^{\text{edt}}, \tau)$ , where  $\epsilon_{\theta}$  represents a parameterized noise predictor network (details in the Appendix Sec. E). A key observation is that the difference in the parameterized noise at the  $n^{\text{th}}$  branch and  $(n-1)^{\text{th}}$  branch is utilized to calculate  $z(n)^{\text{edt}}$  in (4). Finally,  $\epsilon(n)_{\tau}^{\text{cons}}$  is defined by  $\epsilon(n)_{\tau}^{\text{cons}} = (z(n)_{\tau}^{\text{edt}} - \sqrt{\alpha_{\tau}} \dot{z}(n-1)^{\text{edt}}) / \sqrt{1 - \alpha_{\tau}}$ . In contrast to the dual-branch setup proposed by (Xu et al., 2023), where  $z(n)_{\tau}^{\text{edt}}$  is calibrated to a single source branch, our approach calibrates  $z(n)_{\tau}^{\text{edt}}$  to  $\dot{z}(n-1)^{\text{edt}}$ . This means that each  $n^{\text{th}}$  branch is calibrated to its

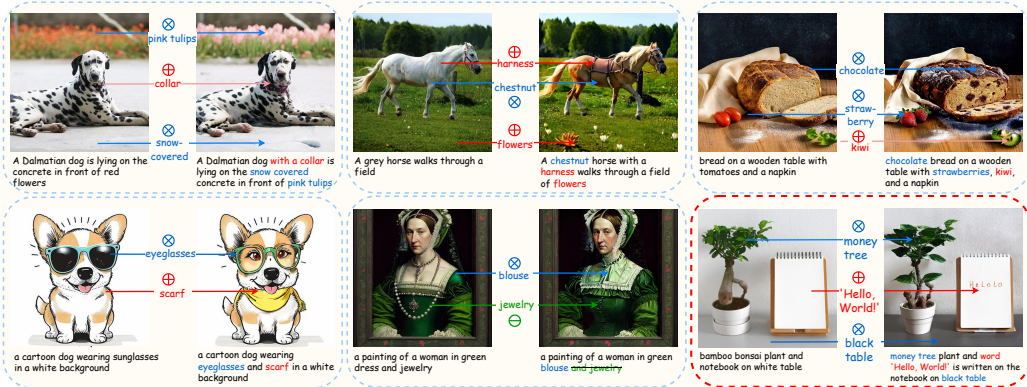


Figure 4: **Qualitative results of MultiEdits.** We denote the edits in arrows with edit actions and aspects for each pair of images. The last image pair is a failure case of MultiEdits.

previous branch. A critical challenge arises when updating all  $N$  branches in parallel:  $z(n-1)^{\text{edt}}$  is not available for updating the  $n^{\text{th}}$  branch. To overcome this challenge, we use the previous time step of  $z(n-1)^{\text{edt}}$ , denoted by  $\dot{z}(n-1)^{\text{edt}}$ , in the computation of  $\epsilon(n)^{\text{cons}}$ .

#### 4.2.3 CROSS-BRANCH INTERACTIONS

For **rigid local branches**, the cross-attention map  $\mathcal{M}_n^i$  from the previous branch is either switched or injected into the current branch, akin to the method used in P2P (Hertz et al., 2022). This approach facilitates local edits while preserving structural consistency. For **non-rigid branch branches**, we observe that the query features in the shallow layers of UNet (Ronneberger et al., 2015) can effectively query correlated local contents and textures from the prior branch’s latent features, ensuring consistency. Consequently, the key and value features from the prior branch are retained in the current branch to maintain consistent editing. We use a non-rigid editing branch to manage non-rigid local edits. In the current branch  $n$ , textures from the previous branch  $(n-1)$  are preserved by replacing the  $K_{n-1}$  and  $V_{n-1}$  features from the last branch with the  $K_n$  and  $V_n$  features in the current branch where the  $K$  and  $V$  are key and query feature from self-attention layer. Only the query features are preserved to maintain layout semantic correspondence. Additionally, the attention mask  $\mathcal{M}_{n-1}$  from the previous branch’s cross-attention layer is used to guide the editing process by adding it to  $\mathcal{M}_n$ , thereby converting the object layout from  $\mathcal{M}_{n-1}$  to  $\mathcal{M}_n$ . This step is crucial for object removal or shape modification edits, where the object mask is derived from the previous branch. For all **global branches**, there is no replacement of attention features or masks, and the attention mask is not used to guide the editing process, as the entire image is intended to be altered.

## 5 EXPERIMENTS

**PIE-Bench++ Dataset.** We introduce a new dataset, PIE-Bench++, derived from PIE-Bench (Ju et al., 2023) and dedicated to evaluate the performance of multi-aspect image editing. The PIE-Bench dataset contains 700 images and prompts with single-aspect editing including object-level manipulations (addition, deletion, or alteration), attribute-level manipulations (changes in content, pose, color, and material), and image-level manipulations that modify background and overall style. Our PIE-Bench++ extends PIE-Bench by enabling multi-aspect edits: 57% of our dataset have two aspect edits per prompt, 19% have more than two edits, and the remaining 24% have a single aspect edit. For additional details and examples of the PIE-Bench++ dataset, please refer to the supplementary material.

**Evaluation Metrics.** We introduce two new metrics designed for evaluating multi-aspect text-driven image editing, alongside standard evaluation metrics.

**(a) Aspect Accuracy-LLaVA.** Drawing inspiration from the remarkable capability of large vision language models in comprehending intricate semantics within images, we propose to innovatively leverage them as an “omniscient” agent equipped with extensive knowledge to understand various attributes of images. We use the LLaVA (Liu et al., 2023) model, trained on visual grounding tasks,

	StyleD	MasaCtrl	P2P	DI	NTI	InfEdit	PnP	DI*	P2P*	InfEdit*	PnP*	Ours
CLIP (%) $\uparrow$	24.02	23.37	24.00	24.40	24.03	24.44	24.90	22.80	25.13	<u>25.17</u>	25.39	<b>25.70</b>
D-CLIP (%) $\uparrow$	8.43	7.68	11.43	<u>13.23</u>	12.08	11.02	11.83	2.74	8.30	11.77	11.85	<b>20.70</b>
Eff. (secs/sample) $\downarrow$	838.17	12.70	33.72	29.70	145.29	<b>2.22</b>	32.51	100.98	121.32	11.82	122.81	<u>4.98</u>
AspAcc-CLIP (%) $\uparrow$	32.37	34.05	26.14	31.95	42.19	42.38	44.91	28.23	38.96	42.38	<u>48.20</u>	<b>51.05</b>
AspAcc-LLaVA (%) $\uparrow$	53.79	55.79	55.04	54.42	59.80	60.55	61.36	46.24	55.21	61.90	<u>63.80</u>	<b>65.19</b>

Table 1: **Comparison results in multi-aspect image editing on the PIE-Bench++ dataset.** Computational efficiency is abbreviated as Eff., and \* denotes the method using sequential editing. The best performance is highlighted in **bold** and the second best performance is underlined.

to evaluate the accuracy of multi-aspect image editing. Given a text prompt with multiple aspects, such as “A [pink] [taxi] with [colorful] [flowers] on top”, we provide the following prompt with the edited image to the LLaVA model: “*Does the image match the elements in [ ]: A [pink] [taxi] with [colorful] [flowers] on top? Return a list of numbers where 1 is matched and 0 is unmatched.*” We then parse the returned list and compute its average to determine the aspect accuracy. We name this new evaluation metric as *AspAcc-LLaVA*. Examples and detailed explanations of this evaluation metric are available in the supplementary material.

**(b) Aspect Accuracy-CLIP.** We also use the similarity of the CLIP (Radford et al., 2021) to evaluate if an attribute has been successfully edited. Given an edited image  $\mathcal{I}_{edt}$  and the target prompt  $\mathcal{P}_{edt}$  with  $k$  edited aspects  $\mathcal{A}_{edt}$ , every time we remove an aspect  $\mathcal{A}_{edt}^j$  from  $\mathcal{P}_{edt}$  and revert it back to  $\mathcal{A}_{src}^i$  as  $\hat{\mathcal{P}}_{edt}$ . We then extract the CLIP (Radford et al., 2021) similarity between the edited image  $\mathcal{I}_{edt}$  and two prompts, i.e.,  $s_1 = CLIP(\mathcal{I}_{edt}, \mathcal{P}_{edt})$  and  $s_2 = CLIP(\mathcal{I}_{edt}, \hat{\mathcal{P}}_{edt})$ . We expect  $s_1 > s_2$  if the aspect  $\mathcal{A}_{edt}^j$  has been successfully edited. Thus, the aspect accuracy is  $\frac{k_s}{k}$  when a total of  $k_s$  aspects have been successfully edited among  $k$  target edits. Note that in the case of an edited or added object that also involves changes in attributes (such as color or material), we consider it a successful edit only if both the object and its attributes have been successfully modified. We name this metric as *AspAcc-CLIP*.

**(c) Standard Metrics.** Several standard metrics widely used for evaluating text-image similarity and image quality are considered, including PSNR, LPIPS (Zhang et al., 2018), MSE, and SSIM (Wang et al., 2004). We also use the CLIP (Radford et al., 2021) score to measure the image-text alignment performance. Additionally, the bi-directional CLIP (D-CLIP) score (Wu & De la Torre, 2022) is reported, which is formulated as follows:

$$\cos(\text{CLIP}_{\text{img}}(\mathcal{I}_{edt}) - \text{CLIP}_{\text{img}}(\mathcal{I}_{src}), \text{CLIP}_{\text{text}}(\mathcal{P}_{edt}) - \text{CLIP}_{\text{text}}(\mathcal{P}_{src}))$$

## 5.1 QUANTITATIVE RESULTS

We first conduct experiment on the PIE-Bench++ dataset to compare our method with the state-of-the-art text-driven image editing methods, including MasaCtrl (Cao et al., 2023), Prompt-to-Prompt (P2P) (Hertz et al., 2022), Plug-and-Play (PnP) (Tumanyan et al., 2023), StyleDiffusion (StyleD) (Wang et al., 2023), Null-text Inversion (NTI) (Mokady et al., 2023), DirectInversion (DI) (Ju et al., 2023), and InfEdit (Xu et al., 2023). An intuitive way to improve off-the-shelf image editing methods is to apply the single-aspect editing method sequentially. We follow (Joseph et al., 2024) to adapt existing image editing methods into sequential editing processes, where these methods are applied multiple times to achieve multi-aspect editing. Each time, only one aspect is edited. Table 1 presents the metrics in terms of text-image similarity (i.e., CLIP and D-CLIP scores), computational efficiency, and aspect accuracy. Our MultiEdits model outperforms all baselines in editing effectiveness, with a slightly longer runtime than the InfEdit model. Even though sequential editing better aligns the target prompt than their vanilla methods, it significantly increases computational overhead and may propagate editing errors over time. Moreover, although the sequential editing is conducted in the latent space, it would introduce more noise and artifacts to the edited image. Hence, their performance in all editing quality metrics was inferior to our method.

## 5.2 QUALITATIVE RESULTS

Fig. 4 presents several examples of our method’s multi-aspect editing on the PIE-Bench++ dataset. The results demonstrate the effectiveness of our method in handling multiple and varied types of edits across diverse image content. Fig. 5 further compares our method with several state-of-the-art models and one popular multi-modal large language model, GPT-4V (OpenAI, 2023), by providing the source image, source prompt, and target prompt to guide the image editing. The Rich-text (Ge et al., 2023) model differs from other models, which uses rich-text prompt to edit the image generated from the plain (source) text prompt. The results show that current image editing models even with sequential editing fail to edit multiple aspects, while multi-modal large

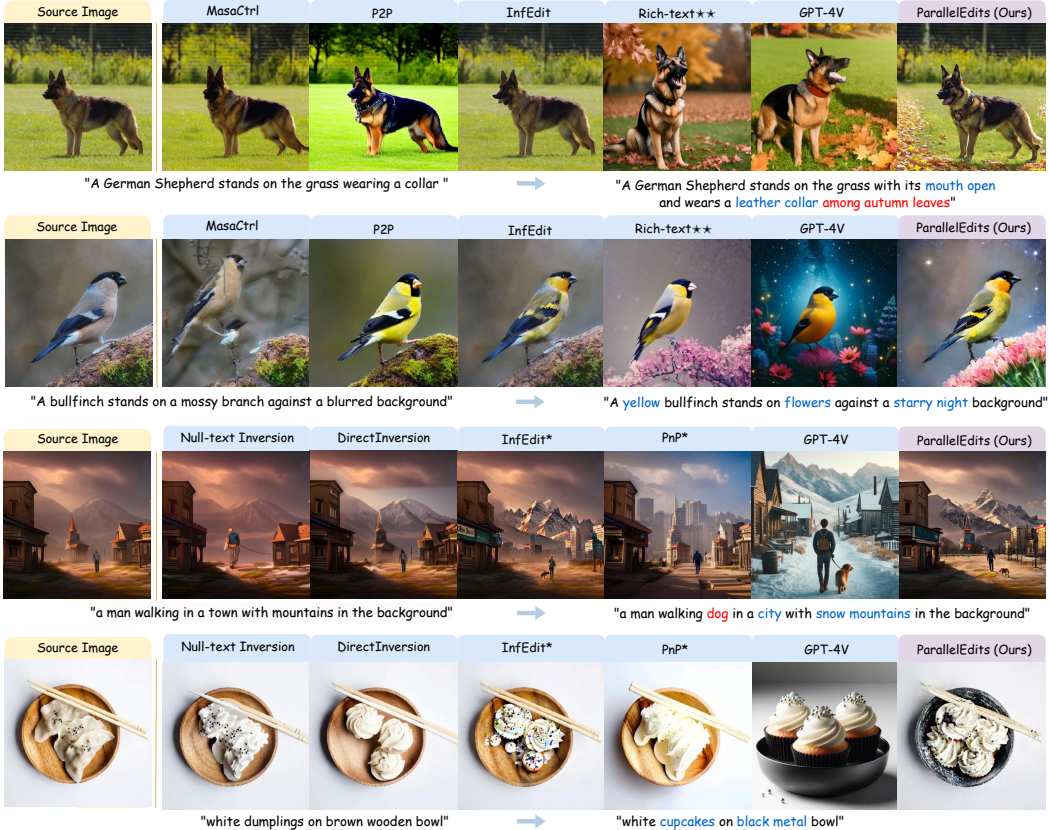


Figure 5: **Qualitative results comparison.** Current methods fail to edit multiple aspects effectively, even using sequential edits (noted as \*). Methods marked with \*\* taking additional inputs other than source image and plain text.

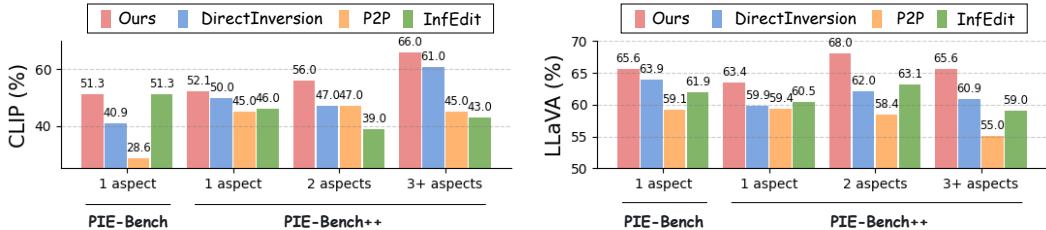


Figure 6: **Comparison across different numbers of editing aspects.** We also include the comparison in PIE-Bench dataset. Our proposed method is robust to different numbers of editing aspects.

language models fail to preserve the content of source image. Our method achieves visually convincing results by successfully editing different attributes with good content preservation.

### 5.3 ABLATION STUDY AND ANALYSIS

**(a) Impact of Editing Aspect Number.** We first examine the performance of our MultiEdits and baseline methods on various editing aspect numbers by comparing CLIP and LLaVA-based aspect accuracies on the original PIE-Bench (Ju et al., 2023) and our PIE-Bench++ datasets. The bar charts in Fig. 6 show the outstanding performance of our method across all settings, including single-aspect editing on two datasets and multi-aspect editing. *Takeaway: the proposed MultiEdits demonstrates robustness across varying numbers of editing aspects.*

**(b) Evaluation on Preservation.** We follow (Ju et al., 2023) to evaluate the background preservation. We first use the PSNR, LPIPS (Zhang et al., 2018), MSE and SSIM (Wang et al., 2004) to evaluate the background preservation. We measure that metric on a subset of images of our proposed PIE-Bench++ dataset where the background can be well defined in that image, e.g., no image style or background editing, and the background is visible after aspect editing. The results are shown in Table 2, where we compare our method with the top performance methods in Table 1. Moreover, we adopt the similar way as calculating the AspAcc-LLaVA to

Methods	Background Preservation				Aspect Preservation %	
	PSNR↑	LPIPS <sub>×10<sup>3</sup></sub> ↓	MSE <sub>×10<sup>4</sup></sub> ↓	SSIM <sub>×10<sup>2</sup></sub> ↑	CLIP↑	LLaVA↑
P2P	18.48 / <b>16.64</b>	188.26 / <b>231.83</b>	190.07 / <b>345.07</b>	73.55 / <b>69.17</b>	20.72 / <b>23.48</b>	66.59 / <b>72.60</b>
PnP	22.73 / <b>21.54</b>	103.16 / <b>120.87</b>	<b>75.97</b> / <b>102.47</b>	80.73 / <b>78.85</b>	20.79 / <b>25.59</b>	75.65 / <b>78.77</b>
InfEdit	24.61 / <b>24.09</b>	103.99 / <b>107.43</b>	160.54 / <b>163.72</b>	78.85 / <b>79.64</b>	24.69 / <b>25.04</b>	75.90 / <b>78.05</b>
Ours	<b>26.13</b>	<b>95.87</b>	113.86	<b>82.35</b>	25.49	<b>80.70</b>

Table 2: **Comparison results in terms of background and aspects preservation.** The results from sequential editing is noted as green. MultiEdits achieves state-of-the-art performance on multi-aspect editing while preserving the background and content consistency.

prompt LLaVA (Liu et al., 2023) for evaluating how the unchanged aspect preserves in the edited image. We also calculate the CLIP (Radford et al., 2021) score between the target image and the text prompt after removing all edited aspects. The results are reported in Table 2 noted as CLIP and LLaVA, respectively. *Takeaway: preservation is even maintained in MultiEdits.*

**Limitations and Failure Cases.** The proposed MultiEdits has several limitations. First, it cannot handle the text editing in the image, as shown in the last image pair of Fig. 4. Second, MultiEdits fails to edit dramatic background changes, as examples shown in the supplementary material.

## 6 CONCLUSION

In this work, we propose a new research task, multi-aspect text-driven image editing, to modify multiple object types, attributes, and relationships. We introduce a dedicated method, MultiEdits, to multi-aspect text-driven image editing as an effective and efficient solution to this problem. Due to the lack of evaluation benchmark, we introduce PIE-Bench++, an improved version of PIE-Bench (Ju et al., 2023) tailored for simultaneous multiple-aspect edits within images. MultiEdits achieves better quality and performance than existing methods on proposed PIE-Bench++. Our work introduces MultiEdits, a novel approach that adeptly handles multiple attribute edits simultaneously, preserving the quality of edits across single and multiple attributes through a unique attention grouping mechanism without adding computational complexity. There are several future works we would like to explore. First, different aspects of an image have a specific semantic order. Editing these aspects according to their intrinsic order will simplify the editing process. Secondly, the current MultiEdits still has limitations, as shown in Fig. 4. It will be of interest to study approaches to improve these aspects.

**Ethics Statement.** In anticipation of contributing to the academic community, we plan to make the dataset and associated code publicly available for research. Nonetheless, we acknowledge the potential for misuse, particularly by those aiming to generate misinformation using our methodology. We will release our code under an open-source license with explicit stipulations to mitigate this risk. These conditions will prohibit the distribution of harmful, offensive, or dehumanizing content or negatively representing individuals, their environments, cultures, religions, and so forth through the use of our model weights.

**Acknowledgement.** This work was supported in part by the National Science Foundation (NSF) Projects under grants SaTC-2153112, No.1822190, and TIP-2137871. Lokhande was supported by UB startup funds. We thank Sudhir Kumar Yaram for the insightful discussions on the project.

---

## REFERENCES

Omri Avrahami, Dani Lischinski, and Ohad Fried. Blended diffusion for text-driven editing of natural images. In *Proceedings of the IEEE/CVF Conference on Computer Vision and Pattern Recognition*, pp. 18208–18218, 2022.

Mingdeng Cao, Xintao Wang, Zhongang Qi, Ying Shan, Xiaohu Qie, and Yinqiang Zheng. Masactrl: Tuning-free mutual self-attention control for consistent image synthesis and editing. In *Proceedings of the IEEE/CVF International Conference on Computer Vision (ICCV)*, pp. 22560–22570, October 2023.

Hangeol Chang, Jinho Chang, and Jong Chul Ye. Ground-a-score: Scaling up the score distillation for multi-attribute editing. *arXiv preprint arXiv:2403.13551*, 2024.

Ting Chen. On the importance of noise scheduling for diffusion models. *arXiv preprint arXiv:2301.10972*, 2023.

Jooyoung Choi, Sungwon Kim, Yonghyun Jeong, Youngjune Gwon, and Sungroh Yoon. Ilvr: Conditioning method for denoising diffusion probabilistic models. *arXiv preprint arXiv:2108.02938*, 2021.

Guillaume Couairon, Jakob Verbeek, Holger Schwenk, and Matthieu Cord. Diffedit: Diffusion-based semantic image editing with mask guidance. *arXiv preprint arXiv:2210.11427*, 2022.

Guillaume Couairon, Jakob Verbeek, Holger Schwenk, and Matthieu Cord. Diffedit: Diffusion-based semantic image editing with mask guidance. In *The Eleventh International Conference on Learning Representations*, 2023.

Ming Ding, Wendi Zheng, Wenyi Hong, and Jie Tang. Cogview2: Faster and better text-to-image generation via hierarchical transformers. *Advances in Neural Information Processing Systems*, 35:16890–16902, 2022.

Songwei Ge, Taesung Park, Jun-Yan Zhu, and Jia-Bin Huang. Expressive text-to-image generation with rich text. In *Proceedings of the IEEE/CVF International Conference on Computer Vision*, pp. 7545–7556, 2023.

Shuyang Gu, Dong Chen, Jianmin Bao, Fang Wen, Bo Zhang, Dongdong Chen, Lu Yuan, and Baining Guo. Vector quantized diffusion model for text-to-image synthesis. In *Proceedings of the IEEE/CVF Conference on Computer Vision and Pattern Recognition*, pp. 10696–10706, 2022.

Amir Hertz, Ron Mokady, Jay Tenenbaum, Kfir Aberman, Yael Pritch, and Daniel Cohen-Or. Prompt-to-prompt image editing with cross attention control. 2022.

KJ Joseph, Prateksha Udhayanan, Tripti Shukla, Aishwarya Agarwal, Srikrishna Karanam, Koustava Goswami, and Balaji Vasan Srinivasan. Iterative multi-granular image editing using diffusion models. In *Proceedings of the IEEE/CVF Winter Conference on Applications of Computer Vision*, pp. 8107–8116, 2024.

Xuan Ju, Ailing Zeng, Yuxuan Bian, Shaoteng Liu, and Qiang Xu. Direct inversion: Boosting diffusion-based editing with 3 lines of code. 2023.

Tero Karras, Samuli Laine, Miika Aittala, Janne Hellsten, Jaakko Lehtinen, and Timo Aila. Analyzing and improving the image quality of stylegan. In *Proceedings of the IEEE/CVF conference on computer vision and pattern recognition*, pp. 8110–8119, 2020.

Tero Karras, Miika Aittala, Timo Aila, and Samuli Laine. Elucidating the design space of diffusion-based generative models. *Advances in Neural Information Processing Systems*, 35:26565–26577, 2022.

Bahjat Kawar, Shiran Zada, Oran Lang, Omer Tov, Huiwen Chang, Tali Dekel, Inbar Mosseri, and Michal Irani. Imagic: Text-based real image editing with diffusion models. In *Proceedings of the IEEE/CVF Conference on Computer Vision and Pattern Recognition*, pp. 6007–6017, 2023.

Siavash Khodadadeh, Shabnam Ghadar, Saeid Motiian, Wei-An Lin, Ladislau Bölöni, and Ratheesh Kalarot. Latent to latent: A learned mapper for identity preserving editing of multiple face attributes in stylegan-generated images. In *Proceedings of the IEEE/CVF Winter Conference on Applications of Computer Vision*, pp. 3184–3192, 2022.

Jizhizi Li, Jing Zhang, and Dacheng Tao. Referring image matting. In *Proceedings of the IEEE/CVF conference on computer vision and pattern recognition*, pp. 22448–22457, 2023.

Tsung-Yi Lin, Michael Maire, Serge Belongie, James Hays, Pietro Perona, Deva Ramanan, Piotr Dollár, and C Lawrence Zitnick. Microsoft coco: Common objects in context. In *European conference on computer vision*, pp. 740–755. Springer, 2014.

Haotian Liu, Chunyuan Li, Qingyang Wu, and Yong Jae Lee. Visual instruction tuning. In *NeurIPS*, 2023.

---

Yuhao Liu, Jiake Xie, Xiao Shi, Yu Qiao, Yujie Huang, Yong Tang, and Xin Yang. Tripartite information mining and integration for image matting. In *Proceedings of the IEEE/CVF International Conference on Computer Vision*, pp. 7555–7564, 2021.

Andreas Lugmayr, Martin Danelljan, Andres Romero, Fisher Yu, Radu Timofte, and Luc Van Gool. Repaint: Inpainting using denoising diffusion probabilistic models. In *Proceedings of the IEEE/CVF Conference on Computer Vision and Pattern Recognition*, pp. 11461–11471, 2022.

Simian Luo, Yiqin Tan, Longbo Huang, Jian Li, and Hang Zhao. Latent consistency models: Synthesizing high-resolution images with few-step inference. *arXiv preprint arXiv:2310.04378*, 2023.

Ron Mokady, Amir Hertz, Kfir Aberman, Yael Pritch, and Daniel Cohen-Or. Null-text inversion for editing real images using guided diffusion models. *arXiv preprint arXiv:2211.09794*, 2022.

Ron Mokady, Amir Hertz, Kfir Aberman, Yael Pritch, and Daniel Cohen-Or. Null-text inversion for editing real images using guided diffusion models. In *Proceedings of the IEEE/CVF Conference on Computer Vision and Pattern Recognition*, pp. 6038–6047, 2023.

Thao Nguyen, Yuheng Li, Utkarsh Ojha, and Yong Jae Lee. Visual instruction inversion: Image editing via image prompting. *Advances in Neural Information Processing Systems*, 36, 2023.

Alex Nichol, Prafulla Dhariwal, Aditya Ramesh, Pranav Shyam, Pamela Mishkin, Bob McGrew, Ilya Sutskever, and Mark Chen. Glide: Towards photorealistic image generation and editing with text-guided diffusion models. *arXiv preprint arXiv:2112.10741*, 2021.

Alexander Quinn Nichol and Prafulla Dhariwal. Improved denoising diffusion probabilistic models. In *International Conference on Machine Learning*, pp. 8162–8171. PMLR, 2021.

OpenAI. Gpt-4v(ision) system card. 2023.

Gaurav Parmar, Krishna Kumar Singh, Richard Zhang, Yijun Li, Jingwan Lu, and Jun-Yan Zhu. Zero-shot image-to-image translation. In *ACM SIGGRAPH 2023 Conference Proceedings*, pp. 1–11, 2023.

Alec Radford, Jong Wook Kim, Chris Hallacy, Aditya Ramesh, Gabriel Goh, Sandhini Agarwal, Girish Sastry, Amanda Askell, Pamela Mishkin, Jack Clark, et al. Learning transferable visual models from natural language supervision. In *International conference on machine learning*, pp. 8748–8763. PMLR, 2021.

Robin Rombach, Andreas Blattmann, Dominik Lorenz, Patrick Esser, and Björn Ommer. High-resolution image synthesis with latent diffusion models. In *Proceedings of the IEEE/CVF Conference on Computer Vision and Pattern Recognition*, pp. 10684–10695, 2022.

Olaf Ronneberger, Philipp Fischer, and Thomas Brox. U-net: Convolutional networks for biomedical image segmentation. In *Medical Image Computing and Computer-Assisted Intervention–MICCAI 2015: 18th International Conference, Munich, Germany, October 5–9, 2015, Proceedings, Part III 18*, pp. 234–241. Springer, 2015.

Jiaming Song, Chenlin Meng, and Stefano Ermon. Denoising diffusion implicit models. *arXiv preprint arXiv:2010.02502*, 2020.

Yang Song, Prafulla Dhariwal, Mark Chen, and Ilya Sutskever. Consistency models. *arXiv preprint arXiv:2303.01469*, 2023.

Raphael Tang, Linqing Liu, Akshat Pandey, Zhiying Jiang, Gefei Yang, Karun Kumar, Pontus Stenetorp, Jimmy Lin, and Ferhan Ture. What the daam: Interpreting stable diffusion using cross attention. *arXiv preprint arXiv:2210.04885*, 2022.

Narek Tumanyan, Omer Bar-Tal, Shai Bagon, and Tali Dekel. Splicing vit features for semantic appearance transfer. In *Proceedings of the IEEE/CVF Conference on Computer Vision and Pattern Recognition*, pp. 10748–10757, 2022.

Narek Tumanyan, Michal Geyer, Shai Bagon, and Tali Dekel. Plug-and-play diffusion features for text-driven image-to-image translation. In *Proceedings of the IEEE/CVF Conference on Computer Vision and Pattern Recognition*, pp. 1921–1930, 2023.

Hao Wang, Guosheng Lin, Ana García del Molino, Anran Wang, Zehuan Yuan, Chunyan Miao, and Jiashi Feng. Maniclip: Multi-attribute face manipulation from text. *arXiv preprint arXiv:2210.00445*, 2022.

Zhizhong Wang, Lei Zhao, and Wei Xing. Stylediffusion: Controllable disentangled style transfer via diffusion models. In *Proceedings of the IEEE/CVF International Conference on Computer Vision*, pp. 7677–7689, 2023.

---

Zhou Wang, Alan C Bovik, Hamid R Sheikh, and Eero P Simoncelli. Image quality assessment: from error visibility to structural similarity. *IEEE transactions on image processing*, 13(4):600–612, 2004.

Chen Henry Wu and Fernando De la Torre. Unifying diffusion models’ latent space, with applications to cyclediffusion and guidance. *arXiv preprint arXiv:2210.05559*, 2022.

Sihan Xu, Yidong Huang, Jiayi Pan, Ziqiao Ma, and Joyce Chai. Inversion-free image editing with natural language. *arXiv preprint arXiv:2312.04965*, 2023.

Sihan Xu, Ziqiao Ma, Yidong Huang, Honglak Lee, and Joyce Chai. Cyclenet: Rethinking cycle consistency in text-guided diffusion for image manipulation. *Advances in Neural Information Processing Systems*, 36, 2024.

Richard Zhang, Phillip Isola, Alexei A Efros, Eli Shechtman, and Oliver Wang. The unreasonable effectiveness of deep features as a perceptual metric. In *Proceedings of the IEEE conference on computer vision and pattern recognition*, pp. 586–595, 2018.

Min Zhao, Fan Bao, Chongxuan Li, and Jun Zhu. Egsde: Unpaired image-to-image translation via energy-guided stochastic differential equations. *Advances in Neural Information Processing Systems*, 35:3609–3623, 2022.

---

## APPENDIX

### A MULTIEDITS: THE ALGORITHM

In this section we provide Algorithm 1: *Early Aspect Grouping* and Algorithm 2: *MultiEdits on a particular branch*. These algorithms describe the overall idea behind MultiEdits. They are also pictorially illustrated in Figures 2 and 3 of the main paper. Let us denote an arbitrary branch and the timestep in the diffusion process by  $n$  and  $t$  respectively. Firstly, in Algorithm 1, we demonstrate how *Early Aspect Grouping* is conducted over the attention maps. Recall that we refer to this as “early” aspect grouping because only a few steps (maximum of 5) are sufficient to perform the grouping. This phase of MultiEdits takes as an input, the edit action set  $\{E^{i \rightarrow j}\}$  and the corresponding cross-attention maps for every token  $\mathbf{A}_{src}^j$ , and outputs the grouped edit actions set  $\bar{\mathcal{A}}_{edt}^c$ . Recall from Section 4 of the paper that  $E^{i \rightarrow j} \in \{\otimes, \oplus, \ominus, \oslash\}$ , with  $\otimes$  denoting a swap action,  $\oplus$  denoting an add action,  $\ominus$  denoting aspect deletion, and  $\oslash$  indicating no change in the aspect. Once grouped edit actions set is computed, it is fed into Algorithm 1 to conduct multi-aspect editing and obtain the edited latent features. In Algorithm 2, we implement several operations on the attention masks, similar to the P2P method (Hertz et al., 2022), and describe them as follows.

**Replace:** Swapping token attention mask  $\mathcal{M}_{n-1}$  in the prompt from previous branch, overriding  $\mathcal{M}_n$ ;

**Refine:** Injecting only the attention mask that corresponds to the unchanged part of the prompt from  $\mathcal{M}_{n-1}$  to  $\mathcal{M}_n$ ;

**Retain:** Keeping the attention mask  $\mathcal{M}_n$  unchanged.

---

#### Algorithm 1 Early Aspect Grouping

---

**Input:** Edit action set  $\{E^{i \rightarrow j}\}$ , Cross attention maps  $\{\mathcal{M}\}$

- 1: rigid-edit  $\leftarrow \{\}$ , non-rigid-edit  $\leftarrow \{\}$ , global-edit  $\leftarrow \{\}$
- 2: **for**  $\mathcal{A}_{edt}^{i \rightarrow j} \in \{E^{i \rightarrow j}\}$  **do**
- 3:     **if**  $\gamma(\bar{\mathcal{M}}_{edt}^j) \geq \beta \gamma(\sum \{\bar{\mathcal{M}}_{edt}\})$  **then** ▷ This is a global edit
- 4:         global-edit  $\leftarrow$  global-edit +  $\{E^{i \rightarrow j}\}$
- 5:     **else if**  $\phi(\bar{\mathcal{M}}_{src}^i, \bar{\mathcal{M}}_{edt}^j) < \lambda$  **then** ▷ This is a non-rigid edit
- 6:         **for**  $\bar{\mathcal{A}}_{edt}^c \in$  non-rigid-edit **do**
- 7:             **if** mIoU( $\bar{\mathcal{A}}_{edt}^c, E^{i \rightarrow j} \geq \lambda$ ) **then** ▷  $\bar{\mathcal{A}}_{edt}^c$  is a set of grouped edit actions
- 8:                  $\bar{\mathcal{A}}_{edt}^c \leftarrow \bar{\mathcal{A}}_{edt}^c + E^{i \rightarrow j}$
- 9:             **else**
- 10:                 non-rigid-edit  $\leftarrow$  non-rigid-edit +  $E^{i \rightarrow j}$
- 11:             **end if**
- 12:         **end for**
- 13:     **else if**  $\phi(\bar{\mathcal{M}}_{src}^i, \bar{\mathcal{M}}_{edt}^j) \geq \lambda$  **then** ▷ This is a rigid edit
- 14:         **for**  $\bar{\mathcal{A}}_{edt}^c \in$  rigid-edit **do**
- 15:             **if** mIoU( $\bar{\mathcal{A}}_{edt}^c, E^{i \rightarrow j} \geq \lambda$ ) **then**
- 16:                  $\bar{\mathcal{A}}_{edt}^c \leftarrow \bar{\mathcal{A}}_{edt}^c + E^{i \rightarrow j}$
- 17:             **else**
- 18:                 rigid-edit  $\leftarrow$  rigid-edit +  $E^{i \rightarrow j}$
- 19:             **end if**
- 20:         **end for**
- 21:     **end if**
- 22: **end for**

**Output:** Grouped edit actions set  $\{\bar{\mathcal{A}}_{edt}^c\}$

---

### B SOME MORE DETAILS ON MULTIEDITS

In the literature (Cao et al., 2023; Hertz et al., 2022), image editing processes have been conducted through the implementation of a dual-branch approach. This method involves utilizing a source and target branches for editing. Specifically, the source branch is reverted to  $z_0$ , while the trajectory of the target branch is iteratively adjusted. By computing the distance from the source branch and  $\epsilon^{\text{cons}}$  with Latent Consistency Model (Song et al., 2023), the target branch is calibrated at each time step.

---

**Algorithm 2** MultiEdits on a Particular Branch

---

**Input:** Denoising UNet  $\varepsilon_\theta$ ,  
 Grouped edit action  $\bar{\mathcal{A}}_{\text{edit}}^c$ , ▷ Output from early aspect grouping  
 Latent feature in previous branch and previous timestep  $z_{n-1}^t, z_n^{t-1}$ ,  
 Cross attention maps  $\{\mathcal{M}\}$ ,  
 Self attention features  $Q_{n-1}, K_{n-1}, V_{n-1}$ ,  
 Edit type list: rigid-edit, non-rigid-edit, global-edit

- 1:  $\mathcal{M}_n \leftarrow \varepsilon_\theta(\bar{\mathcal{A}}_{\text{edit}}^c, z_n^{t-1}, t-1)$
- 2: **if**  $\bar{\mathcal{A}}_{\text{edit}}^c \in \text{global-edit}$  **then** ▷ This is a global edit
- 3:     retain( $\mathcal{M}_n$ ) ▷ Do not switch attention maps for global edits
- 4: **else if**  $\bar{\mathcal{A}}_{\text{edit}}^c \in \text{non-rigid-edit}$  **then** ▷ This is a non-rigid edit
- 5:     replace( $\mathcal{M}_{n-1}, \mathcal{M}_n$ )
- 6: **else if**  $\bar{\mathcal{A}}_{\text{edit}}^c \in \text{rigid-edit}$  **then** ▷ This is a rigid edit
- 7:      $\{Q_n, K_n, V_n\} \leftarrow \{Q_{n-1}, K_{n-1}, V_{n-1}\}$
- 8:     refine( $\mathcal{M}_{n-1}, \mathcal{M}_n$ )
- 9: **end if**
- 10:  $\bar{\mathcal{M}}_n \leftarrow \text{binarize}(\sum_{m=0}^{m \leq n} \mathcal{M}_m)$
- 11:  $z_n^t \leftarrow \bar{\mathcal{M}}_n \odot z_n^t + (1 - \bar{\mathcal{M}}_n) \odot z_{n-1}^t$

**Output:** Latent feature  $z_n^t$

---

	with aspect categorization	with aspect grouping	with auxillary branch	Similarity %		Aspect Accuracy %	
	CLIP↑	D-CLIP↑	CLIP↑	LLaVA↑			
MultiEdits	✗	✗	✗	24.32	10.45	40.97	57.67
	✗	✓	✓	25.14	11.97	46.66	58.37
	✓	✗	✗	24.50	12.33	48.08	61.22
	✓	✓	✓	<b>25.70</b>	<b>20.70</b>	<b>51.05</b>	<b>65.19</b>

Table 3: *Ablation studies on branch numbers and aspect grouping.*

Our experiments, as seen in Section 5 of the main paper, show the ineffectiveness of a dual-branch procedure for multi-aspect editing tasks. Specifically, a single target branch is inadequate, leading to imperfection in the target image. Thereby we advocate multi-aspect editing through the use of multiple target branches. Each target branch handles a group of aspects, with simpler aspects such as non-rigid local edits directed to initial branches, and more complex aspects such as rigid local edits deferred to subsequent ones. Note that however, all the branches operate simultaneously.

**Auxiliary Rigid / Non-Rigid Branches.** In the main paper, it was noted that there was one dedicated branch for each type of edit: non-rigid, rigid, and global edit. The Early Aspect Grouping algorithm 1 classifies aspects into these three categories. Our experiments revealed that sometimes, due to low overlap between attention maps, aspects may not always be grouped into dedicated rigid or non-rigid branches. In such cases, it becomes necessary to include an auxiliary branch to handle the ungrouped aspects. Therefore, MultiEdits may involve a single rigid branch and additional auxiliary branches to manage ungrouped aspects, and similarly, a single non-rigid branch and supplementary auxiliary branches to address ungrouped aspects. An ablation study on auxiliary branches is provided in Table 3.

## C MORE DETAILS ON EVALUATION METRICS

In this section, we describe more details of our evaluation metrics.

**LLaVA aspect accuracy.** We show how we leverage LLaVA (Liu et al., 2023) to evaluate the multi-aspect editing accuracy in Fig. 7 and Fig. 8, we also prompt LLaVA (Liu et al., 2023) for explanation to human readers. LLaVA (Liu et al., 2023) could provide detailed summary for the image and also explanations for the mismatched between edited aspects and image.

**Other evaluation metrics.** Moreover, even though the Structure Distance (Tumanyan et al., 2022) has been used in PIE-Bench (Ju et al., 2023) to evaluate the structure between source and target image while ignoring appearance information, it could not serve as a good evaluation metric for multi-aspect editing. This is due to the fact that the structure of multi-aspect edited target image may necessitate substantial modifications, particularly when it involves adding or removing multiple objects.

User



Does this image match the elements in []:  
 "a [sailboat] is silhouetted against the [evening glow] with [snow] mountain in the backgrounds, [winter scene]."  
 Exactly follow the return format as a list where 1 is matched and 0 is unmatched, return list only.  
 The list length is equal to 4.

LLaVA [1,1,1,1]

Please provide some explanation.

The image matches the elements in the description as follows:

1. A sailboat is present in the image, which is silhouetted against the evening glow.
2. The evening glow is visible in the sky, creating a beautiful backdrop for the sailboat.
3. The mountains in the background are covered with snow, which is consistent with the description.
4. The overall scene is a winter scene, as indicated by the snow-covered mountains and the calm, cold appearance of the water.

Therefore, all elements in the description are matched by the image, resulting in a list of 4 ones.



Does this image match the elements in []:  
 "a man [standing] in a boat is silhouetted against the sunset and [ducks] on the water with [Alps mountain] in the background"  
 Exactly follow the return format as a list where 1 is matched and 0 is unmatched, return list only.  
 The list length is equal to 4.

LLaVA [1,1,1,1]

Please provide some explanation.

The image matches all the elements in the given description:

1. A man is standing in a boat.
2. The man is silhouetted against the sunset.
3. There are ducks on the water.
4. The background features a mountain range, which could be described as Alps-like.

Therefore, the elements in the description are all present in the image, and the list would be [1, 1, 1, 1].



Does this image match the elements in []:  
 "a [boat] in a lake with a [house] and [ice mountain] in the background"  
 Exactly follow the return format as a list where 1 is matched and 0 is unmatched, return list only.  
 The list length is equal to 3.

LLaVA [1,1,1]

Please provide some explanation.

The image shows a boat on a lake with a house and a mountain in the background. The mountain appears to be covered with snow, which could be described as an "ice mountain." The elements in the brackets match the description provided:

A boat is present in the image.  
 A house is visible in the background.  
 The mountain in the background is covered with snow, which could be described as an "ice mountain."

Therefore, the elements in the brackets match the description, and the list would be [1, 1, 1].

Figure 7: **Examples of prompting LLaVA for aspect accuracy measurement in cases of successful editing.** LLaVA can effectively illustrate if and how the target image and edits are misaligned.

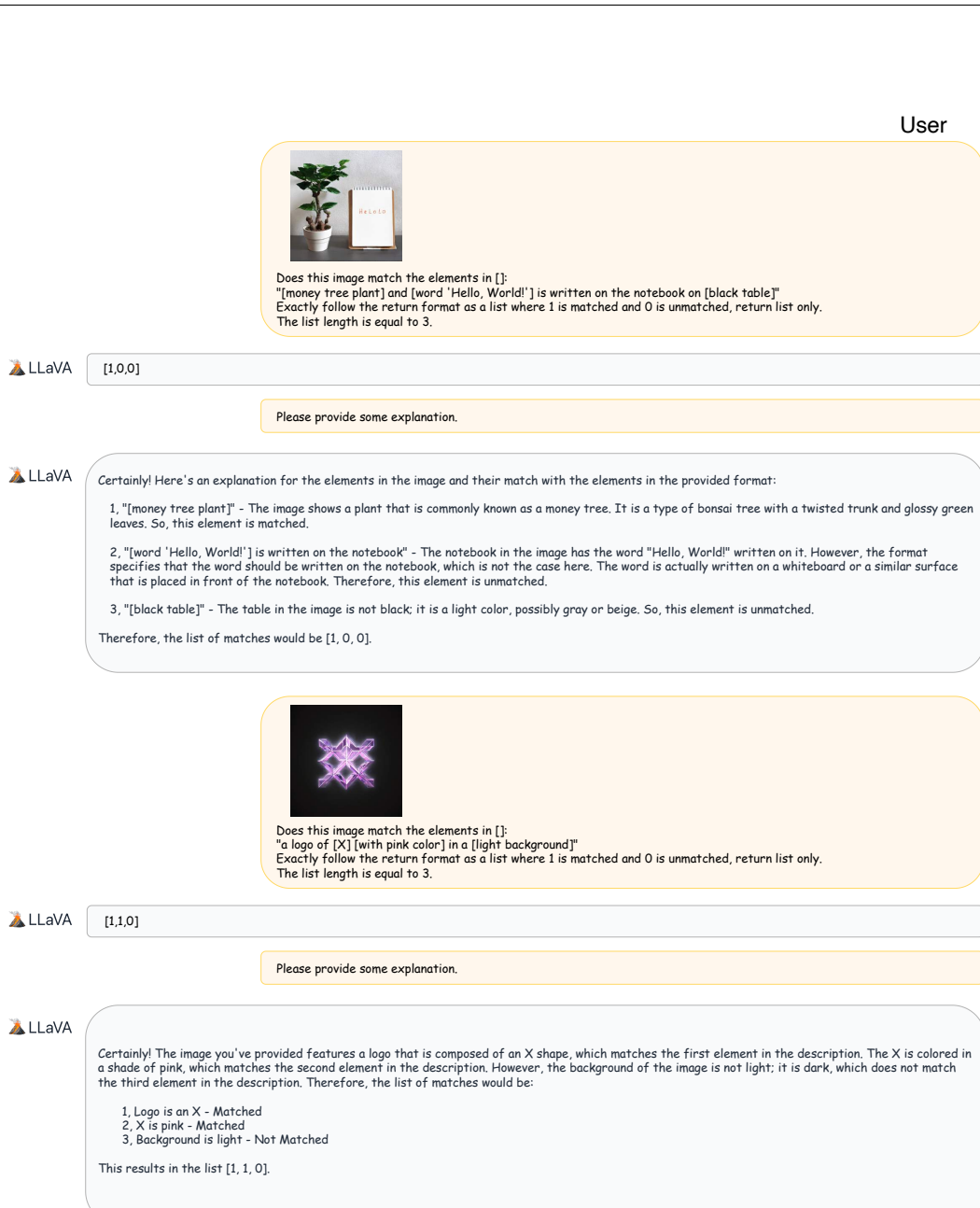


Figure 8: *Examples of prompting LLaVA for aspect accuracy measurement in cases of unsuccessful editing.*

## D ADDITIONAL EXPERIMENTS

**Branches numbers and aspect grouping.** To demonstrate the effectiveness of our multi-branch design and early aspect grouping, we design additional ablation studies for our method in threefold. (1) We only use one single non-rigid branch to conduct all edits; (2) we remove the aspect categorization process from the pipeline and use the same non-rigid branch for each edit; (3) we adopt one single branch for different type of edits without using any auxillary branches which results a total of three branches (also see Section B for more details). As shown in Table 3, the multi-branch design and aspect grouping play a significant role in enhancing the performance of our proposed MultiEdits.

**Performance comparison on each category.** Recall that our dataset includes nine different categories for editing. We compare the performance of baseline models and our approach across the nine categories, as presented in Table 4. Our proposed MultiEdits achieves state-of-the-art performance across most categories.

Aspect Acc-CLIP	Change							Add Object	Delete Object
	Object	Content	Pose	Color	Material	Background	Style		
P2P (Hertz et al., 2022)	33.13	20.00	25.83	34.17	31.67	30.63	19.38	22.29	11.88
MasaCtrl (Cao et al., 2023)	40.83	23.75	<b>40.83</b>	20.00	30.83	26.88	29.38	37.08	28.96
NTI (Mokady et al., 2022)	48.13	41.25	23.75	<u>51.25</u>	24.17	51.25	22.50	40.42	32.08
DirectInversion (Ju et al., 2023)	40.63	26.25	23.33	40.00	25.42	32.50	25.00	30.00	20.83
InfEdit (Xu et al., 2023)	36.24	33.33	25.41	41.67	27.50	48.75	41.88	<u>50.63</u>	<u>45.41</u>
PnP (Tumanyan et al., 2023)	44.38	27.29	27.91	49.17	<u>32.91</u>	<u>52.50</u>	<b>55.63</b>	44.38	42.08
MultiEdits	<b>51.46</b>	<b>44.16</b>	<u>39.58</u>	<b>60.00</b>	<b>47.50</b>	<b>60.00</b>	<u>50.00</u>	<b>56.04</b>	<b>52.08</b>

Table 4: **Comparison on each category in PIE-Bench++.** Our MultiEdits achieves the best performance on most of the categories from the dataset.

## E IMPLEMENTATION DETAILS

Our proposed MultiEdits is based on the Latent Consistency Model (Song et al., 2023), with the publicly available LCM<sup>†</sup> which is finetuned from Stable Diffusion v1.5. We then follow (Xu et al., 2023) to leverage their proposed inversion-free technique in MultiEdits for image editing. During sampling, we perform LCM sampling (Song et al., 2023) with 15 denoising steps, and the classifier-free guidance is set to 4.0. We also set the hyper-parameter  $\theta$  as 0.9 and  $\beta$  as 0.8 in our experiments, where  $\theta, \beta$  are used to determine the edit type of a given edit action.

In the inversion-free multi-branch editing approach, for  $1 < n < N$ , the noise estimation is also conditioned on a text conditioning  $c_n$  in branch  $n$ . This can be expressed as  $e(n)_{\tau}^{\text{edt}} = \epsilon_{\theta}(z(n)_{\tau}^{\text{edt}}, \tau, c_n)$ . Here,  $c_1$  corresponds to the source prompt,  $c_N$  corresponds to the target prompt, and  $c_n$  represents the prompt that includes all aspect edits up to branch  $n$ .

## F ADDITIONAL DETAILS OF PIE-BENCH++

### F.1 PIE-BENCH++ DETAILS

Unlike existing benchmarks that primarily focus on single-aspect edits, PIE-Bench++ is tailored to multiple aspect edits, reflecting the complexities inherent in real-world editing tasks. Our enhanced dataset, PIE-Bench++, builds upon the PIE-Bench (Ju et al., 2023) by incorporating 700 images across nine diverse categories, covering both natural and artificial scenes, with a significant focus on multi-aspect editing scenarios. Specifically, the Change Object category involves swapping objects in the scene with different yet reasonable alternatives. Add Object adds new elements to the scene. Delete Object focuses on removing objects, testing the model’s ability to erase elements seamlessly. Change Object Content alters the content of specific objects, such as changing the design on a shirt or the pattern on a wall. Change Object Pose includes changes in the shape of objects, humans, or animals. Change Object Color assesses the model’s ability to apply accurate color changes. Change Object Material evaluates the rendering of different textures and materials. Change Background involves editing scenarios where there is a distinct foreground object and a main background. This type of edit focuses on seamlessly integrating new background elements while preserving the integrity of the foreground object. Change Image Style involves the application of style transfer techniques to the entire image while ensuring the original content remains intact. For example, this could involve transforming a photograph to adopt a cartoon style. Each category is carefully curated to provide a comprehensive evaluation of the dataset’s multi-aspect editing capabilities, the summary of the dataset is shown in Table 5.

### F.2 DATASET ANNOTATION

The annotation process involves a primary annotator who labels the source prompt, describing the original image, and the target prompt, which outlines the desired modifications to generate the target image. The target prompt is carefully annotated to include all editing operations expected to be reflected in the target image. Subsequently, a second annotator reviews the annotations for accuracy and consistency, ensuring the reliability of the dataset. The majority of target prompts in PIE-Bench++ feature at least two edited aspects. Nevertheless, within the categories that solely changing background and image styles, the number of edits is usually constrained to one or two aspects. This limitation is due to the intrinsic characteristics of these attributes, such as each image having only one background or style.

<sup>†</sup><https://huggingface.co/SimianLuo/LCMDreamshaperv7>

	Change							Add Object	Delete Object
	Object	Content	Pose	Color	Material	Background	Style		
#Edited Aspect	302	98	120	188	99	112	165	178	119
#Edited Token	316	155	227	205	116	175	424	507	381

Table 5: **Summary of Editing Types and Categories in PIE-Bench++ dataset.** There are 10 different categories in PIE-Bench++ and a total number of 700 images.

**Annotation format details.** Each image in the dataset annotation is associated with key elements as shown in Fig. 9: a source prompt, a target prompt, an edit action, and a mapping of aspects. The edit action specifies the position index in the source prompt where changes are to be made, the type of edit to be applied, and the operation required to achieve the desired outcome. The aspect mapping connects objects undergoing editing to their respective modified attributes, enabling the identification of which objects are subject to editing.

Source Image	Text-based annotation
	<pre> "source_prompt": "a colorful bird standing on a branch", "target_prompt": "a brown owl standing on a red flower", "edit_action": {"owl":{"position":2,"edit_type":1,"action":"bird"}, "brown":{"position":1,"edit_type":6,"action":"colorful"}, "flower":{"position":6,"edit_type":1,"action":"branch"}, "red":{"position":6,"edit_type":6,"action": "+"}}, "aspect_mapping": {"owl":["brown"],"flower":["red"]} </pre>
	<pre> "source_prompt": "the galaxy over the durdle door", "target_prompt": "the pink sunset and rainbow over the durdle door", "edit_action": {"pink":{"position":1,"edit_type":6,"action": "+"}, "sunset":{"position":1,"edit_type":8,"action":"galaxy"}, "and rainbow":{"position":2,"edit_type":2,"action": "+"}}, "aspect_mapping": {"sunset":["pink"],"rainbow":[]} </pre>
	<pre> "source_prompt": "a slanted mountain bicycle on the road in front of a building", "target_prompt": "a slanted rusty mountain motorcycle on the road in front of a fence", "edit_action": {"rusty":{"position":2,"edit_type":7,"action": "+"}, "motorcycle":{"position":3,"edit_type":1,"action":"bicycle"}, "fence":{"position":11,"edit_type":8,"action":"building"}, "on the road":{"position":4,"edit_type":3,"action": "-"}}, "aspect_mapping": {"motorcycle":["rusty"],"fence":["red"],"road":[]} </pre>
	<pre> "source_prompt": "a round cake with orange frosting on a wooden plate", "target_prompt": "a square cake with strawberry frosting on a plastic plate", "edit_action": {"square":{"position":1,"edit_type":4,"action":"bird"}, "strawberry frosting":{"position":4,"edit_type":6,"action":"orange frosting"}, "plastic":{"position":8,"edit_type":7,"action":"wooden"}}, "aspect_mapping": {"cake":["square","strawberry frosting"],"plate":["plastic"]} </pre>

Figure 9: **Annotation examples from PIE-Bench++.** Each annotation containing a Source Prompt, Target Prompt, Edit Action, and Aspect Mapping. Edit action contains the specific instructions including the desired modification index in source prompt as position, edit type among 9 categories and the action  $\in \{\otimes, \oplus, \ominus\}$ . The aspect mapping indicates the pair between object and attribute.

## G ADDITIONAL QUALITATIVE RESULTS

We also provide more qualitative results in Fig. 10, showing the effectiveness of our proposed method in handling multi-aspect editing tasks. These examples showcase the model’s proficiency in executing intricate edits. For instance, as depicted in Fig. 10 (b), our method successfully removes a cup while accurately reconstructing the obscured parts of the lamp behind it. In Fig. 10 (a), the model demonstrates its ability to swap and add aspects, while preserving the composition of the scene. The results underscore the model’s adeptness in interpreting and executing sophisticated editing instructions, leading to visually consistent and contextually fitting edited images.

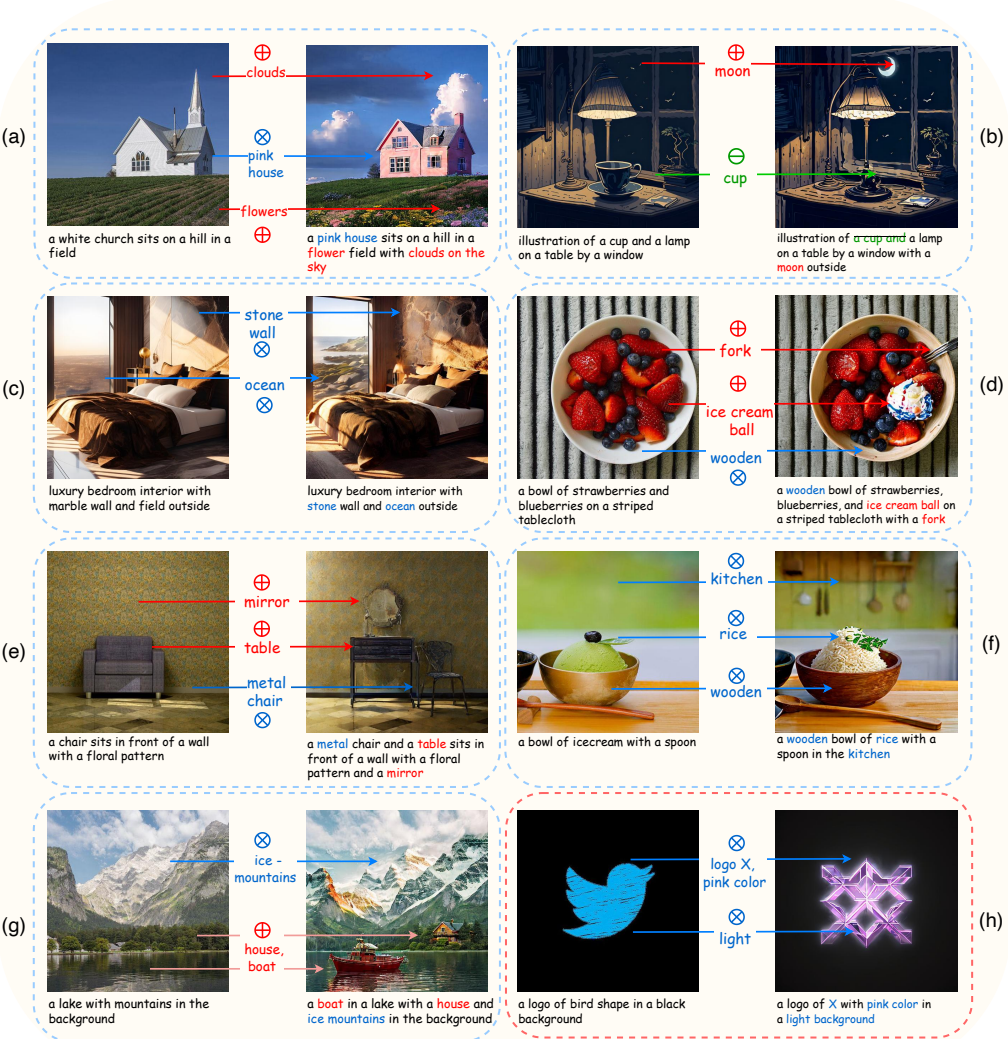


Figure 10: *Qualitative results from MultiEdits*. MultiEdits is able to swap, add and delete multiple aspects. The last image pair is a failure case of MultiEdits.